Strain-coupling and relaxation dynamics in multicaloric ammonium sulphate (NH4)2SO4

Michael Carpenter, Miguel Costa, Guillaume Nataf, Xavier Moya

Editors' Suggestion

Strain-coupling and relaxation dynamics in multicaloric ammonium sulphate $(NH_4)_2SO_4$

Michael A. Carpenter [1,*] Miguel B. Costa [2] Guillaume F. Nataf [3] and Xavier Moya [2]

[1]Department of Earth Sciences, University of Cambridge, Downing Street, Cambridge CB2 3EQ, United Kingdom
[2]Department of Materials Science and Metallurgy, University of Cambridge, 27 Charles Babbage Road, Cambridge CB3 0FS, United Kingdom
[3]GREMAN—UMR 7347, CNRS, Université de Tours, INSA CVL, 37000 Tours, France

(Received 24 April 2023; accepted 5 June 2023; published 11 August 2023)

Ammonium sulphate $(NH_4)_2SO_4$ (AS) has recently been shown to display giant barocaloric and electrocaloric effects when its paraelectric-ferrielectric transition at ∼225 K is driven by hydrostatic pressure or an electric field, respectively. Important aspects of the structural evolution in this context are coupling of strain to molecular librational modes, distortions, and rotations of NH_4^+ and SO_4^{2-} groups, and to changes in hydrogen bonding. Resonant ultrasound spectroscopy (RUS) has been used to reveal subtle elastic and anelastic relaxation processes of single crystals of AS through the temperature interval 5–300 K that are indicative of (i) coupling of strain to the driving order parameter, modified by a transformation microstructure, and (ii) of hysteretic effects that are attributed to different dynamics of displacive and order/disorder components of the phase transition. At high temperatures, partial chemical decomposition results in the formation of triammonium hydrogen disulphate $(NH_4)_3H(SO_4)_2$ (AHS) which displays elastic and anelastic anomalies associated with phase transitions at ∼265, 139, 132, and 72 K. Freezing of defects coupled with strain occurs at temperatures below ∼35 K in both AS and AHS.

DOI: 10.1103/PhysRevMaterials.7.083601

I. INTRODUCTION

Ammonium sulphate (AS) is an inorganic salt that has traditionally enjoyed wide use as a soil fertilizer and more recently has been classed as a multicaloric material [1]. Caloric materials display nominally reversible thermal changes in response to changes of a ferroic order parameter driven by an applied field, and they could help combat climate change by underpinning heat pumps that obviate the need for greenhouse gases [2,3]. Multicaloric materials can be driven simultaneously or sequentially by more than one type of applied field and may lead to, for example, wider ranges of operating temperature and elimination of hysteresis in one control parameter by transferring it to another [1].

Pressure-driven isothermal changes in entropy of $\sim 60\,JK^{-1}\,kg^{-1}$ in response to small pressure changes of ∼0.1 GPa were reported for AS [4], and electric-field-driven isothermal changes in entropy of $\sim 30\,J\,K^{-1}\,kg^{-1}$ in response to large electric field changes of $400\,kV\,cm^{-1}$ were reported in the same material [5]. The existence of giant barocaloric effects and electrocaloric effects near the ferrielectric phase transition in a material that is easy to synthesize and is made from cheap abundant elements has brought renewed focus on the fundamental understanding of AS.

Earlier interest in AS was stimulated by the discovery of a complex electrostructural phase transition at ∼225 K [6–8]. The symmetry change is orthorhombic to orthorhombic, $Pnam \leftrightarrow Pna2_1$, and the transition is pseudoproper ferrielectric [9–11] on the basis that the driving order parameter is not the electrical polarization but a structural change that has the same symmetry as the polarization [12]. As summarized by Malec *et al.* [13] and Meijer *et al.* [14], the structural changes can be described in terms of displacements and distortions of two symmetrically distinct NH_4^+ groups, rotations of SO_4^{2-} groups, and changes in the configuration of hydrogen bonds. A longstanding issue in this context relates to whether the transition is primarily displacive or order/disorder in character. Based on recent simulations and diffraction experiments, Malec *et al.* [15] concluded that the transition has a mixed character. By way of contrast, Yuan *et al.* [16] concluded that the large entropy change at the transition can be explained by considering librational modes only, without contributions from configurational changes.

The focus of this paper is on the thermomechanical properties of AS. Resonant ultrasound spectroscopy (RUS) has been used to investigate the coupling of strain to librational modes, distortions, and rotations of NH_4^+ and SO_4^{2-} groups, and to changes in hydrogen bonding across the ferrielectric phase transition. The most characteristic feature of the complete RUS dataset between 10 and 300 K is hysteresis in resonance frequencies between cooling and heating. We propose that this is indicative of different kinetic constraints on relaxations involving order/disorder and hydrogen bonding, as opposed to purely displacive effects. In addition, there may be a contribution from changing net piezoelectric coefficients of bulk samples, depending on the configuration of ferrielectric

*mc43@esc.cam.ac.uk

domains. Heating to ~485 K results in partial decomposition of AS to $(NH_4)_3H(SO_4)_2$ (AHS), which displays elastic and anelastic anomalies associated with an additional set of phase transitions.

The most straightforward starting point for characterization of strain relaxation phenomena in AS is to consider a single order parameter coupled with strain (Sec. II). Spontaneous strain variations determined from analysis of published lattice parameter data do not match those of a classical phase transition with one order parameter, however, and it is necessary to invoke the additional influence of an order parameter arising from the ferroelastic transition which occurs at higher temperatures (Sec. III). A comprehensive set of elastic and anelastic properties determined from acoustic resonance spectra of millimeter-sized single crystals is presented in Sec. IV.

II. PHASE TRANSITIONS, ORDER PARAMETERS, AND STRAIN COUPLING

Based on symmetry alone and using the software package ISOTROPY [17], the zone center phase transition between structures with space groups *Pnma* and $Pna2_1$ has a one-component order parameter q with the symmetry of irreducible representation Γ_4^-. This is equivalent to the B_{1u} order parameter used in the literature, where the transition is expressed in terms of the alternative setting of *Pnma* as $Pnam \rightarrow Pna2_1$. Coupling of components of the strain tensor e_1-e_6 with the order parameter can be expressed in the simplest possible Landau free energy expansion as

$$\begin{aligned} G = {} & \tfrac{1}{2}a(T-T_c)q^2 + \tfrac{1}{4}bq^4 + \tfrac{1}{6}cq^6 + (\lambda_1 e_1 + \lambda_2 e_2 + \lambda_3 e_3)q^2 \\ & + \left(\lambda_4 e_4^2 + \lambda_5 e_5^2 + \lambda_6 e_6^2\right)q^2 + \tfrac{1}{2}\left(C_{11}^{o} e_1^2 + C_{22}^{o} e_2^2 + C_{33}^{o} e_3^2\right. \\ & \left. + C_{44}^{o} e_4^2 + C_{55}^{o} e_5^2 + C_{66}^{o} e_6^2\right) + C_{12}^{o} e_1 e_2 \\ & + C_{13}^{o} e_1 e_3 + C_{23}^{o} e_2 e_3. \end{aligned} \tag{1}$$

Only the linear strains e_1, e_2, and e_3, along the crystallographic x, y, and z directions respectively, have nonzero values in the low-temperature structure. Shear components e_4, e_5, and e_6 are strictly zero. Here, T is temperature, T_c is the critical temperature, a, b, and c are standard Landau coefficients, λ_i's are coupling coefficients, and $C_{ij}^{o\prime}$s are the bare elastic constants, i.e., excluding any influence of the phase transition. Application of the equilibrium condition $\partial G/\partial e_i = 0$ leads to the expectation that each of e_1, e_2, and e_3 will scale with q^2 in the usual way (e.g., Ref. [18]). Strong coupling with the linear strains drives the transition to become first order by renormalization of the fourth-order coefficient b, as in the well-known case of quartz [19].

AS is an improper ferroelastic because of a hexagonal-to-orthorhombic transition, $P6_3/mmc$-*Pnam*, at higher temperatures. The transition occurs at ~745 and ~860 K in isomorphous K_2SeO_4 and K_2SO_4, respectively [20–22], and is most likely to have been responsible for an anomaly in the heat capacity of AS near 643 K when a pressure of 100 bar was applied to suppress decomposition [23]. Crystals grown at temperatures within the stability field of the orthorhombic structure of each of these phases can contain ferroelastic twins as growth defects or as a consequence of mechanical deformation [22,24–26]. The order parameter for the ferroelastic transition q_{fs} has the symmetry of an irreducible representation belonging to the M point of the Brillouin zone of space group $P6_3/mmc$. The symmetry-breaking shear strain of the orthorhombic structure with respect to the parent hexagonal structure e_o can be expressed in terms of the lattice parameters of the former without serious loss of precision as

$$e_o = \frac{2(b-\sqrt{3}c)}{(b+\sqrt{3}c)}. \tag{2}$$

This couples with q_{fs} as $\lambda e_o q_{fs}^2$. Coupling between the two order parameters q and q_{fs} is biquadratic $\lambda_q q^2 q_{fs}^2$.

If the ferrielectric transition has an order/disorder component related to the orientations of NH_4^+ or SO_4^{2-} molecules, the order parameter for this contribution q_{od} would have the same symmetry as q. Coupling between the displacive and order/disorder contributions would be bilinear $\lambda q q_{od}$ [27]. The temperature dependence of equilibrium values of q and q_{od} would then be expected to follow solutions of a generalized Landau expansion:

$$\begin{aligned} G = {} & \tfrac{1}{2}a(T-T_c)q^2 + \tfrac{1}{4}bq^4 + \tfrac{1}{2}a_{od}(T-T_{c,od})q_{od}^2 \\ & + \tfrac{1}{4}b_{od}q_{od}^4 + \lambda q q_{od}. \end{aligned} \tag{3}$$

If the two critical temperatures T_c and $T_{c,od}$ are identical, only one order parameter is needed, and q and q_{od} would be linearly dependent. If the critical temperatures are different, there would still be only one symmetry-breaking transition point, but the individual variations of q and q_{od} would be more complex, and spontaneous strains would not follow the classic pattern seen for phase transitions with a single order parameter. This does not take account of the fact that relaxation kinetics of the two order parameters might be sufficiently different for equilibrium values of q_{od} not to be maintained in a given experiment.

III. STRAIN ANALYSIS

Spontaneous strain variations have been investigated here using the combined lattice parameter data of Shmyt'ko *et al.* [28] and Lloveras *et al.* [4], which display a discontinuity at the transition temperature $T_{tr} \sim 225$ K (Fig. 1). Lattice parameters given in Fig. 8 of Asahi *et al.* [29] show temperature dependences that are closely similar to these. Reference parameters $a_o(T)$, $b_o(T)$, and $c_o(T)$, representing lattice parameters of the parent (*Pnam*) structure, were obtained by fitting a function of the form $x_o(T) = x_1 + x_2\Theta_s\coth(\Theta_s/T)$ to the data above T_{tr} (following, for example, Refs. [30,31]). A value of $\Theta_s = 205$ K was obtained from fitting to the combined data for unit cell volume in the temperature interval 229–359 K [Fig. 1(d)]. This was then held fixed in the fitting of a_o, b_o, and c_o [Figs. 1(a)–1(c)]. Values of the individual strains were calculated as $e_1 = (a-a_o)/a_o$, $e_2 = (b-b_o)/b_o$, and $e_3 = (c-c_o)/c_o$ and are shown in Fig. 2(a). The volume strain V_s was taken as $e_1 + e_2 + e_3$ [Fig. 2(b)]. Variations of the orthorhombic shear strain e_o are shown in Fig. 2(c).

Each of e_1 and e_2 display smooth increases in magnitude with falling temperature below the discontinuity at T_{tr}, as would be expected for a classical phase transition with first-order character described by Eq. (1). However, e_3 and

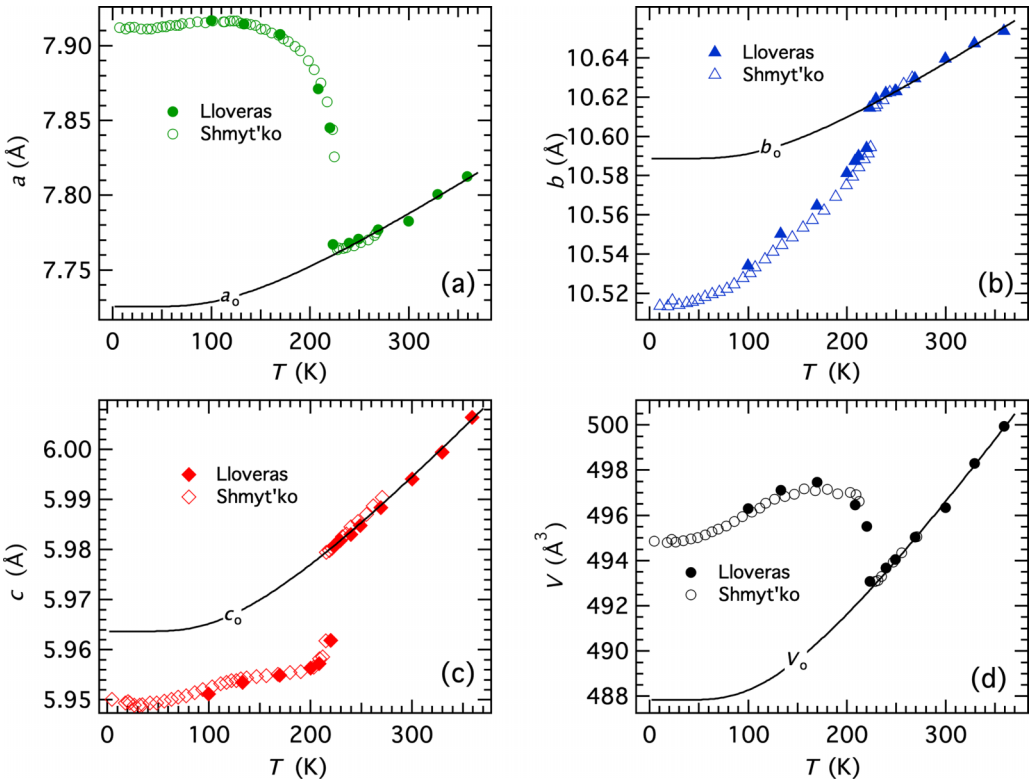

FIG. 1. Combined lattice parameter data of Shmyt'ko *et al.* [27] and Lloveras *et al.* [4]. Curved lines are fits of the function $x_o = x_1 + x_2\Theta_s\coth(\Theta_s/T)$ to the combined data between 229 and 359 K. Extrapolation to low temperatures gave values of the reference parameters a_o, b_o, c_o, and V_o. The value of $\Theta_s = 205$ K from the fit to the unit cell volume data was used in fits for $a_o(T)$, $b_o(T)$, and $c_o(T)$.

V_s initially increase before decreasing, suggesting either that coupling terms that are higher order in q than those in Eq. (1) are significant or that there is an additional order parameter. One candidate for this is q_{fs} due to the hexagonal-orthorhombic transition. Values of e_o are in the range 2–2.5% [Fig. 2(c)] and show a reversal of trend with falling temperature below the discontinuity at T_{tr}. This implies that q_{fs} increases with falling temperature at $T > T_{tr}$ but decreases at $T < T_{tr}$ and hence that the biquadratic coupling between q and q_{fs} is unfavorable. There will also be a volume strain coupled with q_{fs}^2, and if this is positive (increasing V_s with increasing q_{fs}^2), it will contribute to the observed reduction in values of V_s as q_{fs} becomes progressively more suppressed.

IV. RUS

A. Experimental methods

RUS is an established technique for measuring elastic and anelastic properties of samples with dimensions in the range ~0.1–5.0 mm [32]. Values of the elastic moduli scale with the square of the frequencies f of natural resonances of the sample. The inverse mechanical quality factor Q^{-1} provides a measure of acoustic loss. Facilities in Cambridge allow spectra to be collected routinely in the frequency range 0.1–2 MHz at temperatures between ~1.5 and 1500 K and have been described elsewhere [33–35]. Values of f and the peak width at half maximum height Δf are obtained by fitting individual resonance peaks in the primary spectra with an asymmetric Lorentzian function. Values of Q^{-1} are taken as $\Delta f/f$.

AS single crystals were prepared in stages. A white precipitate was obtained by mixing two equivalents of ammonium hydroxide and one equivalent of sulfuric acid in water. The precipitate was dissolved in water, which was then allowed to evaporate at room temperature over a few days to yield millimeter-sized transparent single crystals. Individual crystals are identified below by numbers: Crystal #2 (11.1 mg), Crystal #3 (8.6 mg), Crystal #4 (4.1 mg), Crystal #5 (8.5 mg), Crystal #8 (10.0 mg), and Crystal #9 (12.4 mg).

B. Fracture

Giant barocaloric materials display large volume strains when they are driven using pressure, and this can lead to fracture in brittle materials such as polycrystalline $MnCoGeB_{0.03}$ [36], for example. In past studies of AS, it has been reported that cooling and heating through the ~225 K transition can result in the development of extensive cracking [7,37–40]. RUS provides a convenient method for detecting the development of cracks and, hence, also for identifying pathways that do not lead to fracture. This is particularly relevant for electrocaloric applications, where fracture leads to failure. By contrast, barocaloric effects in powders can be driven via pressure-transmitting media, and the large surface area in a powdered sample is conducive to heat transfer [36]. In this paper, we confirm that slow thermal cycling does not compromise the mechanical integrity of AS single crystals.

The consequences of crack development on cooling through the transition at ~225 K in AS are seen clearly in stacks of RUS spectra collected during cooling and

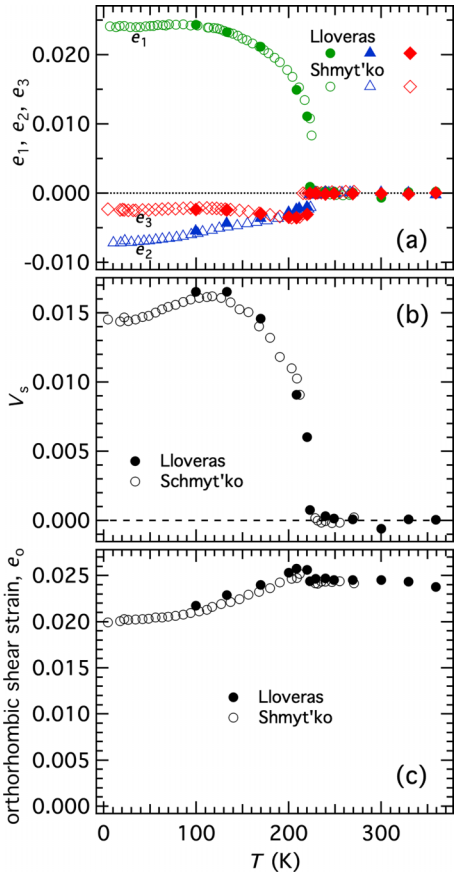

FIG. 2. Spontaneous strains calculated from the lattice parameters shown in Fig. 1. (a) Linear strains. (b) Volume strain. (c) Orthorhombic shear strain. The volume strain was calculated as $e_1 + e_2 + e_3$. Values of e_o were calculated using Eq. (2).

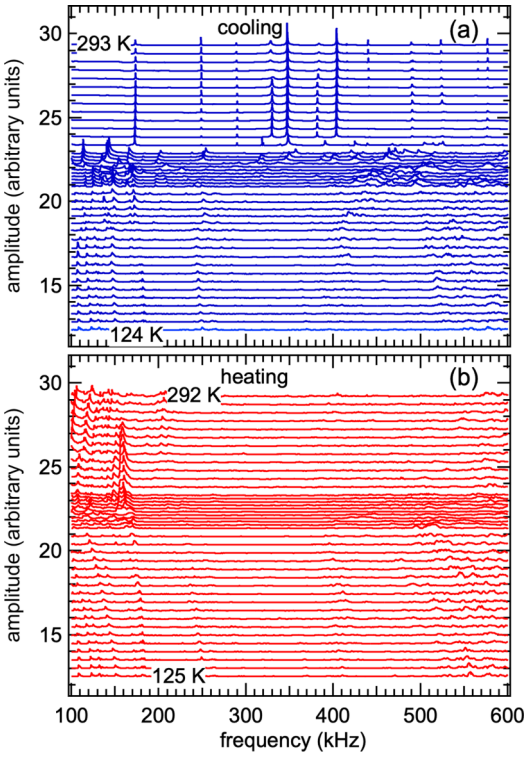

FIG. 3. Resonant ultrasound spectroscopy (RUS) spectra from single Crystal #9, stacked up the y axis in proportion to the temperatures at which they were collected. The cooling sequence (a) was in ∼5 K steps from room temperature to ∼228 K, ∼2 K steps to ∼208 K, ∼5 K to ∼125 K, and the reverse for subsequent heating (b). A settle time of 15 min was used to allow for thermal equilibration before data collection at each set point. Spectra were collected using DRS Modulus II electronics, with a voltage of ±25 V to the driving transducer in an Orange helium flow cryostat. Liquid nitrogen was used for cooling. The sample chamber had been evacuated and then filled with a few millibars of helium gas at the start.

subsequent reheating of a single crystal in Fig. 3. During cooling in steps of ∼5 K down to ∼229 K and in ∼2 K steps from ∼228 to 222 K, discrete peaks typical of the normal acoustic resonances of a mechanically robust sample were present. These shifted to lower frequencies, indicative of elastic softening, as the transition was approached. Individual spectra collected both during further cooling to ∼124 K and during heating back to room temperature contained a very different pattern of more numerous and much weaker peaks. A thermal equilibration period of 15 min was included before data collection at each set point. The crystal emerged intact but with multiple cracks which must have been initiated during cooling through the transition.

As has been found by Hussinger and Unruh [38], it is possible to devise experimental strategies that limit the development of cracking arising from the phase transition. In this paper, it was found that a slower cooling/heating rate prevented any overt mechanical failure from occurring. Figure 4 shows stacks of spectra collected in the Teslatron cryostat with 5 K steps through the interval 295–240 K, 1 K steps through the interval 240–210 K, and 5 K steps down to 190 K. The thermal equilibration period was 20 min before data collection at each set point. Not only did the pattern of discrete resonance peaks remain after cooling through the transition point, but on reheating to room temperature, the spectra contained the same pattern of resonances as at the start.

C. Elastic softening/stiffening and anelastic loss

Linear-quadratic coupling terms of the form $\lambda e q^2$ in Eq. (1) would be expected to result in softening of elastic constants below the transition point with the temperature dependence shown in Fig. 5(a) for a weakly first-order transition (following Fig. 5(i) of Ref. [41]). Biquadratic terms such as $\lambda e^2 q^2$ will give stiffening (or softening, depending on the sign of λ) which scales with q^2 and should have the form illustrated in Fig. 5(b) (following Fig. 5(r) of Ref. [41]). In the case of the weakly first-order hexagonal-trigonal transition in quartz, for example, C_{11}, C_{33}, C_{12}, and C_{13} follow the pattern of Fig. 5(a), and C_{44} follows the pattern of Fig. 5(b) [24].

Due to material-specific dynamical effects, additional softening may occur as the transition point is approached from above [41]. This additional softening should be restricted to elastic constants that transform, in the group theoretical sense, as the identity representation of the space group of the high-symmetry phase. In the case of quartz, C_{44} and C_{66} show little or no precursor softening, while C_{11}, C_{12}, C_{13}, and C_{33} all show softening.

Previously reported variations of the elastic moduli and elastic compliances of AS fit broadly with these expectations, though with only limited softening above T_{tr} [37,42–45].

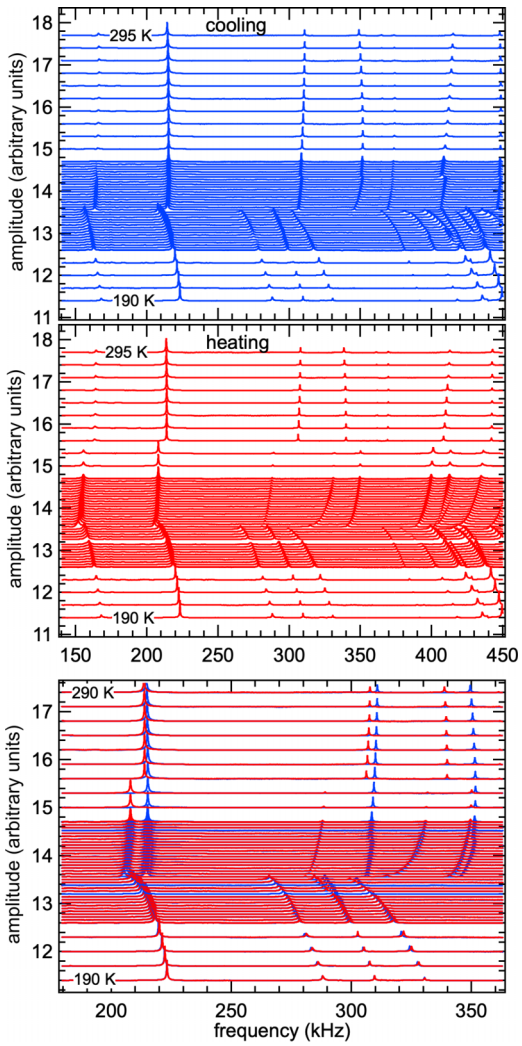

FIG. 4. Resonant ultrasound spectroscopy (RUS) spectra from Crystal #2, stacked up the y axis in proportion to the temperatures at which they were collected. Each spectrum contained 50 000 data points in the frequency range 50–1200 kHz. The cooling sequence was 295–245 K in 5 K steps, 245–210 K in 1 K steps, 210–190 K in 5 K steps, and the same in reverse for heating. The settle time before data collection at each set point was 20 min. At the start, the sample chamber had been evacuated and then filled with 1 bar helium. Spectra collected during cooling (blue) and during heating (red) are shown together over a slightly narrower frequency interval in the bottom panel to illustrate hysteresis.

The frequencies of individual acoustic resonances are determined by combinations of elastic moduli which depend predominantly on shearing. Note that, because the shape and orientation of crystal faces of the as-grown crystals was unspecified, it was not possible to determine absolute values of the elastic constants. However, as shown for the variations of representative resonances in Fig. 6, patterns of softening/stiffening can be compared with the two patterns in Fig. 5. Variations of f^2 in Figs. 6(b) and 6(c) match the pattern of Fig. 5(a) ($\lambda e q^2$ coupling), while the variations in Figs. 6(a) and 6(d) resemble more nearly the pattern shown in Fig. 5(b) ($\lambda e^2 q^2$ coupling). Other resonances display patterns consisting of mixtures of the two.

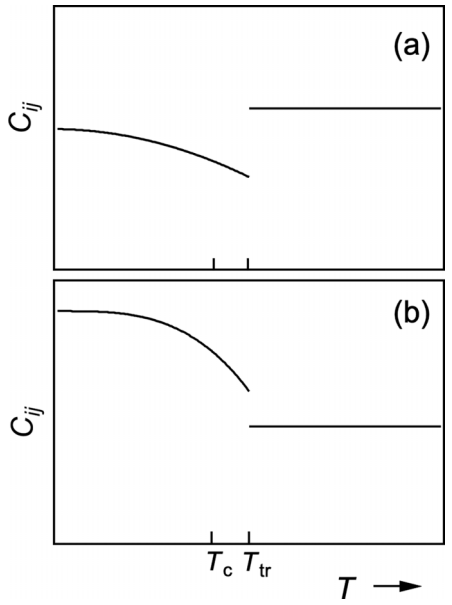

FIG. 5. Schematic variation of elastic constants expected for a first-order coelastic transition (after Ref. [41]). T_c is the critical temperature, T_{tr} is the transition temperature. (a) C_{ij}, $i, j = 1-3$, due to coupling of the form $\lambda e_i q^2$. (b) C_{ii}, $i = 4-6$, due to coupling of the form $\lambda e_i^2 q^2$.

The transition point is taken to be the temperature at which a steep change in resonance frequencies occurred. This is between 225 and 226 K during both cooling and heating of Crystal #2, between 225 and 226 K during cooling and between 226 and 227 K during heating for Crystal #4, between 224 and 226 during cooling and between 227 and 228 K during heating for Crystal #3, and between 224 and 225 K during cooling and between 225 and 226 K during heating for Crystal #8.

Figure 6 shows that, in addition to the expected patterns of softening/stiffening attributable to coupling of the driving order parameter with strain, there are unexpected hysteresis effects. Specifically, variations of f^2 during cooling and heating were essentially the same below the transition point but markedly different between the transition point and ~260 K. The frequencies of some resonances returned to their original values at room temperature [Figs. 6(a) and 6(d)], while small offsets remained in others [Figs. 6(b) and 6(c)]. All resonance frequencies showed marked differences between cooling and heating in the temperature interval ~225−260 K, with an abrupt offset between 255 and 260 K during heating. Some but not all resonances showed offsets: near 239 K during cooling of Crystal #2 and near 237 K during cooling of Crystal #4. A relatively small example of this is indicated by the red arrow in Fig. 6(d). Crystal #8 showed the same patterns, except that the small offsets during cooling occurred near 230 K and the offsets during heating occurred between 260 and 265 K.

Variations of acoustic loss are shown as variations in Q^{-1} in Fig. 6. For most resonances, the transition was marked by a peak at T_{tr}. Values of Q^{-1} were generally higher immediately below T_{tr} than at temperatures well above T_{tr} and decreased with falling temperature below T_{tr} in a manner that was reversed during heating. They displayed hysteresis above T_{tr},

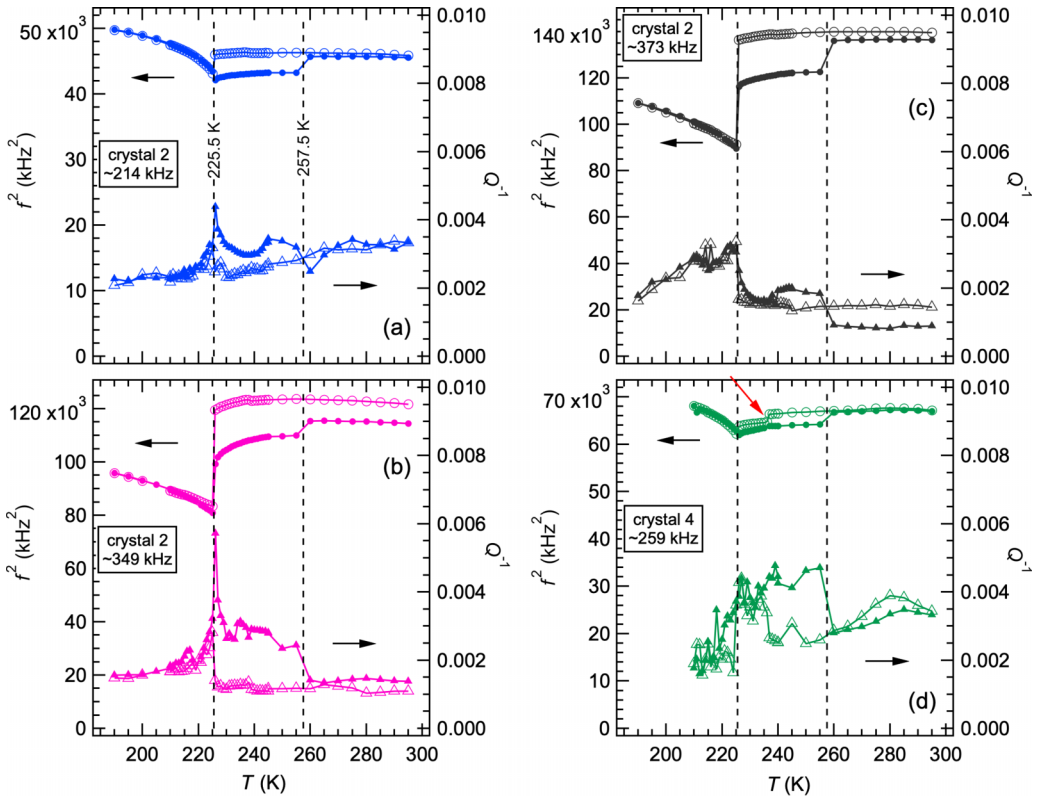

FIG. 6. Variations of f^2 and Q^{-1} from fitting of representative peaks in resonance spectra collected during a sequence of cooling and subsequent heating, with steps of 1 K through the transition point. Values in kilohertz given in the inserts indicate the approximate frequency of each resonance near room temperature. Open symbols represent cooling, and filled symbols represent heating; circles are f^2, triangles are Q^{-1}. (a)–(c) Crystal #2. Cooling down to 190 K, followed by heating. (d) Crystal #4. Cooling down to 210 K, followed by heating. The red arrow in (d) is included to draw attention to a small offset in f^2 values near 239 K during cooling.

retaining relatively high values in the interval ∼225−255 K during heating before reducing abruptly at ∼260 K to values more nearly the same as during initial cooling. There are also clear correlations of small step changes in Q^{-1} at temperatures away from T_{tr} where there are step changes in f^2, i.e., at ∼258 K during heating of Crystal #2 [Figs. 6(a)–6(c)] and at ∼235 K during cooling of Crystal #4 [red arrow in Fig. 6(d)].

D. Cycling to low temperatures

Crystals #2 and #4 were reloaded into the cryostat to follow their elastic properties down to 5 K. The step size through the transition point was again 1 K. Variations of f^2 and Q^{-1} of representative resonance peaks from the primary spectra are given in Fig. 7, along with data for peaks with similar frequencies in spectra collected in the first cycle. Remounting crystals invariably means that different resonances are excited but still allows effective comparison of the main trends in successive cycles.

Principal features of the second cycles to 5 K are, firstly, a distinct hysteresis in f^2 values between cooling and heating above ∼30−40 K. Below this interval, the f^2 values are essentially coincident, but above it, they diverge. There is no indication that the change is due to a discrete phase transition, and it is likely to be indicative of freezing of some aspect of the structure or microstructure. Any peak in acoustic loss which might be due to a Debye-like freezing process is below the level of sensitivity of Q^{-1} variations, however. Secondly, variations of f^2 above T_{tr} during heating from 5 K are markedly different from the pattern shown by heating in the first cycle and cooling in both cycles. Finally, Q^{-1} values are generally higher above T_{tr} during heating in the second cycle.

There appears to be no evidence in the elasticity data of additional phase transitions. There are no overt anomalies in the vicinity of 90 K when the net electric polarization of AS goes to zero, consistent with the interpretation of this point being due simply to a crossover of opposing electric polarization of two sublattices in a ferrielectric structure [8,10]. Schmyt'ko *et al.* [28] proposed that an incommensurate structure is stable between 225 and ∼170 K in AS, but no evidence has been found in this paper for a phase transition at ∼170 K. If there was a stability field for the incommensurate structure, there should be an elastic anomaly at the incommensurate ↔ $Pna2_1$ transition, as has been seen at ∼93 K in the analogous transition sequence of K_2SeO_4 [46,47].

The assembled data in Figs. 6 and 7 indicate that the elastic properties of single crystals of AS vary with the thermal history to which they have been subjected. While it is not possible to rule out definitively the development of microcracks, the recovered crystals did not show any obvious cracks when examined in polarized light or between crossed polars.

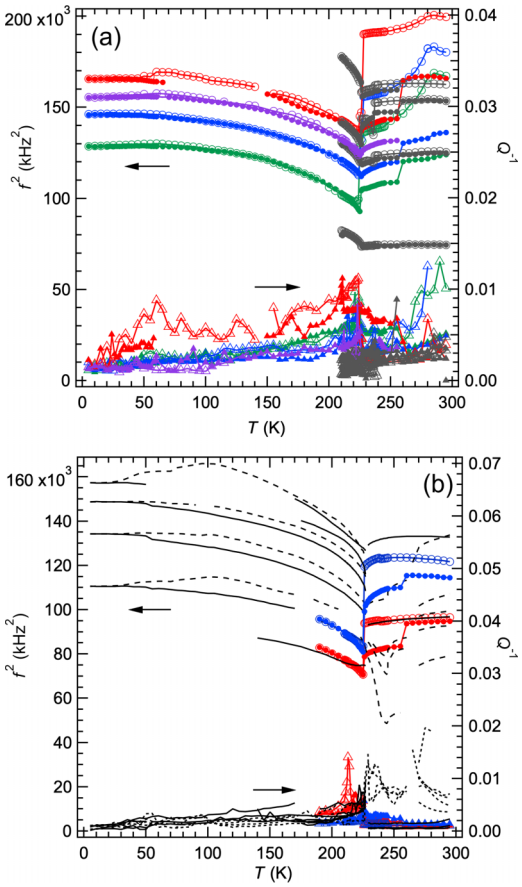

FIG. 7. Variations of f^2 and Q^{-1} from fitting of selected resonance peaks with frequencies in the range ∼250−450 kHz collected in separate cooling/heating cycles from (a) Crystal #4 and (b) Crystal #2. The first cycle was down to 210 K for Crystal #4 and down to 190 K for Crystal #2. The second cycle was down to 5 K. Data are plotted differently in (a) and (b) to allow features common to both to be seen. In (a), data for the first cycle are shown in dark gray. Data for resonance peaks from the second cycle are shown in color: open symbols = cooling, filled symbols = heating. In (b), data for two resonances from the first cycle are shown in color: open symbols = cooling, filled symbols = heating. Data for resonance peaks in spectra collected in the second cycle are shown as black lines: solid lines = cooling, broken lines = heating. Abrupt changes in resonance frequencies occurred during heating through T_{tr} in the second cycle so that it is not possible to identify how peaks below T_{tr} correlated with peaks above T_{tr}.

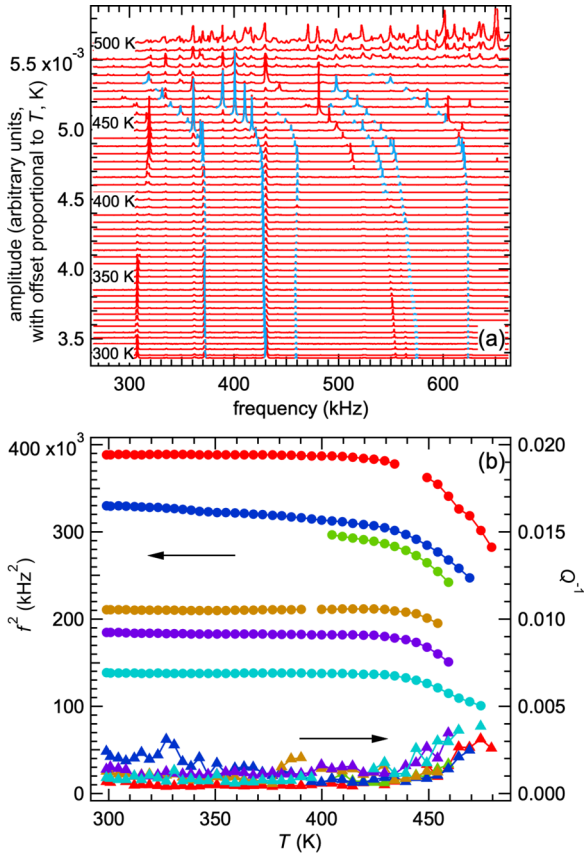

FIG. 8. Resonant ultrasound spectroscopy (RUS) data collected during heating from room temperature to 500 K in steps of ∼5 K for Crystal #5. Each spectrum contained 65 000 points in the frequency interval 100–1200 kHz. (a) Segments of the primary spectra, stacked up the y axis in proportion to the temperature at which they were collected. Blue curves are fits to resonance peaks from the sample which can be observed in spectra collected at temperatures up to ∼480 K. Severe degradation of the sample is indicated by the increase in the number of peaks in spectra collected at ∼485 K and above. (b) Variations of f^2 and Q^{-1} from fits shown in blue in (a). Note that there are no obvious anomalies in the vicinity of 415 K. A trend of steeper softening with increasing temperature accompanied by a trend of increasing Q^{-1} started at ∼440 K.

E. Cycling to high temperatures

Figure 8(a) contains RUS spectra collected during heating of Crystal #5 from room temperature up to 500 K in steps of ∼5 K, with a settle time of 15 min before data collection at each set point. Resonance peaks with frequencies that did not vary with temperature were from the alumina buffer rods. Resonance peaks from the sample showed smooth decreases in frequency through the full temperature interval up to ∼480 K but could not be followed to higher temperatures. Spectra collected at ∼485 K contained many more small peaks, signifying substantial mechanical degradation of the sample. Variations of f^2 and Q^{-1} from fits to selected peaks marked in blue in Fig. 8(a) are shown in Fig. 8(b). The softening trend of f^2 values with increasing temperature became steeper above ∼440 K. The onset of this trend of steeper softening was accompanied by increases in Q^{-1}. The data show no evidence for any discrete phase transition or Debye-like acoustic loss between room temperature and 480 K.

Variations of f^2 and Q^{-1} are shown in Fig. 9 for representative resonance peaks in spectra collected from Crystal #10 during two heating/cooling cycles above room temperature. A step size of ∼2 K was used at the highest temperatures, with an upper limit of 455 K chosen to limit mechanical degradation. f^2 data for the first heating sequence show the same smooth variations with increasing temperature as seen in Fig. 8(b) for Crystal #5. They then display marked hysteresis during cooling, with initial softening rather than stiffening followed by a steplike increase in f^2 at ∼416 K. Room-temperature values at the end were lower than at the start. f^2 data for the second cycle show an abrupt step at ∼416 K

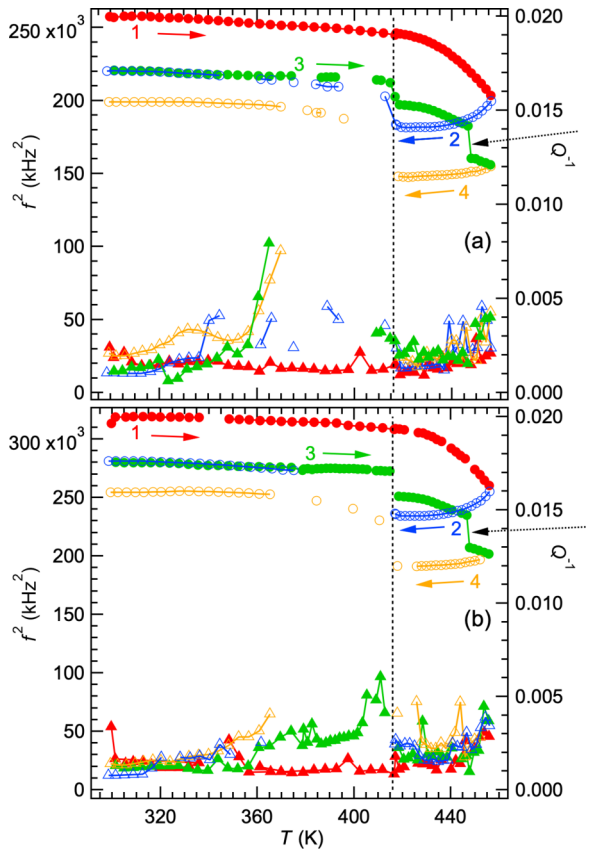

FIG. 9. Variations of f^2 (circles) and Q^{-1} (triangles) from fitting of two representative resonance peaks in spectra collected in successive heating/cooling cycles from Crystal #10. The full sequence involved heating to 455 K (1, filled red circles, triangles), cooling back to room temperature (2, open blue circles, triangles), reheating to 455 K (3, filled green circles, triangles), cooling back to room temperature (4, open orange circles, triangles). The vertical dotted line at 416 K marks the temperature at which a steplike anomaly occurred in each of the heating/cooling sequences apart from the first heating sequence. Black dotted arrows indicate a steplike softening that occurred during the second heating sequence when the computer hung up for 12 h with the sample sitting at 447 K. Data for Q^{-1} for cooling cycles are not shown in the interval 380–416 K because resonance peaks from the sample were too weak to be fit.

during both heating and cooling but again did not return to original room-temperature values. Individual peaks were generally sufficiently well defined to yield reliable values of Q^{-1} for the heating sequences and at temperatures $<\sim$375 K or $>\sim$416 K in the cooling sequences. Resonance peaks from the sample became broad and barely detectable immediately on cooling through 416 K.

The absence of any anomaly in elastic properties near 415 K during the first heating sequence, followed by a reversible anomaly at about this temperature during cooling and in subsequent heating/cooling cycles, mimics the behavior reported by Song *et al.* [48] and Kim *et al.* [49] for the appearance of anomalies in dielectric properties measured at frequencies between 0.5 kHz and 13 MHz. This shows that a degree of decomposition of the sample to other phases occurred at the highest temperatures, as has been characterized more fully in the literature (e.g., Refs. [50–53]). Additional steep reductions in f^2 values, indicated by the black dotted arrows in Fig. 9, occurred between 447 and 448 K when the experiment hung up for ∼12 h with the sample at 447 K. This is attributed directly to progressive decomposition, as is the overall degree of irreversible softening between heating and cooling.

The mass of Crystal #10 at the end of the heating/cooling cycles was 11.5 mg. Assuming an experimental uncertainty of ±0.1 mg, the reduction in mass of 0.3 ± 0.2 implies a weight loss of between ∼1 and ∼4%. The initial crystal was translucent and had a well-defined extinction position when viewed between crossed polars in an optical microscope. While it remained mechanically robust and retained its original shape, the sample at the end was white rather than translucent and had a mosaic of fine cracks across its surface. Between crossed polars, it displayed a white birefringence color without going to extinction in any orientation, qualitatively similar to the images shown in Fig. 3 of Lee *et al.* [52] of a single crystal of AS heated to 473 K. Partial decomposition of AS to an aggregate of fine-grained material had taken place.

F. Cycling to low temperatures following high-temperature treatment

As summarized by Muroyama *et al.* [53] and Kosova *et al.* [23], possible product phases of the decomposition of AS due to heating in air include $(NH_4)_3H(SO_4)_2$ (AHS), NH_4HSO_4, and $NH_4SO_3NH_2$. Each of these phases has different transitions that might be used to provide a fingerprint of which phase(s) developed in Crystal #10 during cycling up to 455 K. The sample in its partially decomposed state was therefore returned to the low-temperature instrument. Data for f^2 and Q^{-1} from fitting of the lowest-frequency peak in spectra collected in a full cooling/heating cycle down to 10 K are shown in Fig. 10. A second cooling/heating sequence was between 305 and 235 K.

Steep softening by 80–90% occurred between ∼265 and ∼180 K in the first cooling sequence [Fig. 10(a)]. Smaller degrees of softening are evident at ∼135 and ∼70 K, with leveling off below ∼50 K [Fig. 10(c)]. Here, Q^{-1} values in Fig. 10(b) show a small increase below ∼250 K followed by the same steep increase through 225 K, as seen previously for the ferrielectric phase transition in AS [e.g., in Fig. 7(a)]. There is a weak rounded peak at ∼135 K and a peak between ∼70 and ∼10 K which has a maximum value at ∼40 K.

Smaller temperature steps were used for data collection during the first heating sequence to provide better resolution through the intervals in which anomalies were seen during cooling. The most obvious feature, however, is the hysteresis in f^2 variations which returned to lower values at all temperatures above ∼35 K [Figs. 10(a) and 10(c)]. The form of distinct anomalies in the temperature dependence of f^2 is also different, but the temperatures at which they occurred ∼72, ∼139, and 225 K are close to their temperatures during cooling. There are no clear anomalies in f^2 or Q^{-1} ∼265 K during heating. By way of contrast, the variations of Q^{-1} match more closely the variations obtained for cooling, at least up to 225 K [Fig. 10(b)]. Above 225 K, they are significantly higher than the values obtained for cooling. The small peak centered at ∼135 K in the cooling data has a sharp

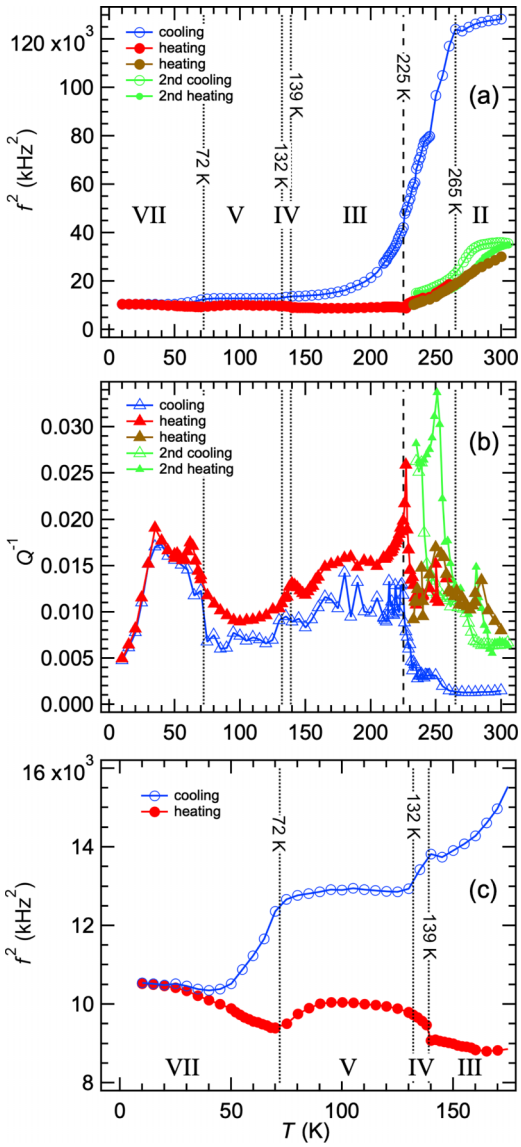

FIG. 10. (a) f^2 and (b) Q^{-1} data from fitting of the resonance peak with lowest frequency in resonant ultrasound spectroscopy (RUS) spectra collected during cooling and reheating of Crystal #10 through the temperature interval 10–300 K after completion of the measurements above room temperature shown in Fig. 9. Data for two resonances with frequencies which almost overlap in the primary spectra from the first heating sequence are shown in red and brown. A vertical dashed line at 225 K marks the expected temperature of the ferrielectric transition in ammonium sulphate (AS). Dotted lines mark anomalies in the temperature dependence of f^2 at ∼265, ∼139, ∼132, and ∼72 K. (c) Enlarged view of the f^2 data in (a) showing details of anomalies below 170 K. Roman numerals represent a tentative assignment of the structures to the sequence summarized by Sohn *et al.* [62].

maximum at 139 K in the heating data. The lowest-temperature peak gave sharp maxima at 35 and 62 K in the heating sequence. Below ∼35 K, results for cooling and heating are indistinguishable.

Data from the second cooling/heating sequence show that f^2 and Q^{-1} values remained close to those observed in the first heating sequence rather than showing any tendency to recover to values seen in the first cooling sequence [Figs. 10(a) and 10(b)]. They have nonlinear softening with falling temperature and a hysteretic offset of ∼10−15 K between temperatures at which the steepest changes occurred on approaching room temperature. The pattern of changes in Q^{-1} was like that shown in the first heating sequence but offset to higher temperatures.

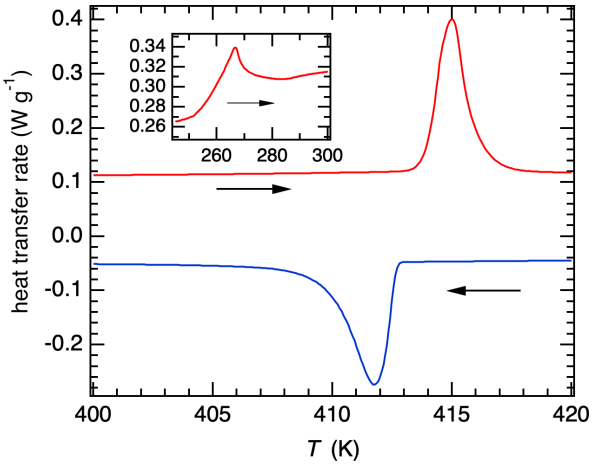

FIG. 11. Calorimetric data for Crystal #10, after the end of all resonant ultrasound spectroscopy (RUS) measurements, collected in a TA Instruments Q2000 differential scanning calorimeter at a heating and cooling rate of 5 K min^{-1}. Arrows indicate the direction of temperature change. There are narrow peaks at 415.0 (endothermic during heating) and 411.8 K (exothermic during cooling), typical of a first-order transition. The insert shows a smaller anomaly at ∼267 K, measured during heating, with a form more typical of a thermodynamically continuous transition. The two anomalies occur at temperatures which correspond with known transitions in $(NH_4)_3H(SO_4)_2$.

A peak in Q^{-1} and a small step in f^2 values at ∼225 K correspond with the ferrielectric transition in AS. They signify that the sample had not transformed completely to other phases. AHS has a sequence of structures with transitions originally reported to be at 63, 133, 141, 265, and 413 K [54,55]. More recent studies have refined some of the details or have proposed additional transitions (e.g., Refs. [56–62]), but the elastic anomalies reported here in Figs. 9 and 10 occur at temperatures which match at least four of the known transitions.

Confirmation of two transformations at ∼268 and ∼413 K is provided by calorimetric data collected from Crystal #10 after the end of all RUS measurements. Figure 11 shows steep peaks at 415 and 412 K during heating and cooling, respectively, at a rate of 5 K min^{-1}. Heating and cooling rates of 20 and 40 K min^{-1} gave a larger hysteresis interval for this first-order transition but the same average temperature for the peak 413 K. The small difference from 416 K for the anomalies in f^2 and Q^{-1} is presumed to represent an offset in the calibration of temperature in the high-temperature RUS instrument. The form of the smaller peak in calorimetric data at ∼268 K (insert in Fig. 11) is more nearly characteristic of a transition which is thermodynamically continuous.

$NH_4SO_3NH_2$ melts congruently at 406 K [23]. Calorimetric data revealed a distinct phase transition at 255 K but no

evidence of further transitions down to 8 K [63]. There is a small anomaly in Q^{-1} in the first cooling sequence at ~255 K, which may or may not be significant in suggesting the presence of a small amount of $NH_4SO_3NH_2$ in the decomposed fraction of Crystal #10.

Another possible decomposition product NH_4HSO_4 melts incongruently to sulfuric acid and AHS at 417 K according to Kosova *et al.* [23] and has structural phase transitions at 263 and 150 K [64]. Other measurements of physical properties by Diosa *et al.* [65] and Björkström *et al.* [66] indicate transition temperatures of ~154 and ~270 K. Mikhaleva *et al.* [67] found 165 and 273 K. There are no obvious anomalies in the elastic data at ~150−170 K shown in Fig. 10(c), so NH_4HSO_4 can probably be ruled out as a major component of the partially decomposed crystal.

V. DISCUSSION

Changes in elastic properties accompanying the pseudoproper ferrielectric transition in AS conform qualitatively to the expectations of conventional strain/order parameter coupling at a weakly first-order phase transition. There are differences, however, including nonclassical evolution of the spontaneous strains [Figs. 2(a) and 2(b)] and marked hysteresis between heating and cooling such that the observed elastic properties are sensitive to the thermal history of the sample (Figs. 6 and 7). The simplest explanation of the differences is that they arise from coupling of properties with more than one order parameter. Nonequilibrium variations can then develop if different order parameters respond to changing temperature with different kinetics. Hysteresis effects may arise also from irreversible changes in microstructure with thermal history. Different combinations of values of the order parameters and/or different domain configurations would lead to different values of the elastic moduli and/or piezoelectric coefficients.

A. Multiple order parameters

For the situation that the ferroelastic and ferrielectric transition mechanisms are purely displacive, the two order parameters q_{fs} and q should maintain equilibrium values down to the lowest temperatures. On the basis of extrapolation of data from electron paramagnetic resonance (EPR) spectra from SeO_4 present as a dopant in AS, an estimate of the ferroelastic ($P6_3/mmc$-$Pnam$) transition temperature is 585 K [68], somewhat below the anomaly in heat capacity observed ~643 K by Kosova *et al.* [23]. The difference of 360 or 418 K from 225 K for the ferrielectric transition means that the coupling between q and q_{fs} will not be as strong as if the critical temperatures were close. Evidence that coupling between q and q_{fs} is unfavorable was presented above as the change in trajectory of the orthorhombic shear strain at the transition point [Fig. 2(c)]. In addition, while evolution of coupled order parameters for two displacive transitions could account for the temperature dependence of the spontaneous strains, it is not likely to account directly for the hysteretic effects.

Bilinear coupling of two order parameters with different critical temperatures and different kinetics has been thoroughly investigated for an analogous phase transition in the mineral albite ($NaAlSi_3O_8$) [69–72], where q is displacive and q_{od} relates to ordering of Al and Si between tetrahedral sites. Their evolution is strongly interdependent, but the evolution of q is different from equilibrium when followed at different fixed values of q_{od}. In the case of AS, q arises from a librational mode [16,73–76]. A thermally activated step for q_{od} depends on the kinetics of changes in hydrogen bonding associated with evolving configurations of NH_4^+ or SO_4^{2-} molecules. The increase in Q^{-1} immediately below the transition point [Fig. 7(a)] most likely arises from an acoustic loss process that involves coupling of strain with local dynamical switching between orientations at relaxation times on the order of $\sim 10^{-5}$–10^{-6} s. This timescale falls within the range of correlation times for rotation of NH_4^+ groups below the transition point determined from nuclear magnetic resonance spectroscopy, which also yielded an activation energy of ~0.04 eV [77].

If local configurations that developed over longer periods during cooling did not all relax back to the same configurations during heating, the evolution of the acoustic resonance frequencies would show hysteretic effects due to small differences in spontaneous strain and/or to changes in net piezoelectric coefficients. On this basis, nonequilibrium evolution of NH_4^+ and SO_4^{2-} orientations provides a possible explanation of the differences between cooling and heating in the interval ~30−225 K seen in Figs. 6 and 7. The observation that acoustic resonances were the same during heating and cooling below ~30 K [Figs. 7(b) and 10(c)] suggests that there is a freezing temperature for changes in hydrogen bonding below which q evolves at constant q_{od}.

Cooling through the ferrielectric transition resets the configurations of NH_4^+ and SO_4^{2-}. Failure to return to the original configuration on reheating back into the stability field of the paraelectric structure would account for the hysteretic variations of f^2 seen in the temperature interval ~225−260 K. In other words, there is some local structure or microstructure immediately above the transition point which is paraelectric on average but depends in detail on thermal history. Resonance frequencies returned to essentially the same values during heating as observed during cooling when the temperature reached 260 K, consistent with q_{od} becoming able to then relax back to equilibrium values.

Equivalent kinetic effects seem to be important in the development of cracks during relatively fast cooling through the transition point. Slow cooling in steps of 1 or 2 K/h allows time for adjustment of both q and q_{od} in such a way that shear and volume strains can be accommodated in a single crystal without cracking. During faster cooling, the cracks develop because of more abrupt changes in strain coupled with relaxation of q on a faster time scale than relaxation of q_{od}.

B. Microstructures

Hysteresis of physical properties well away from a transition point often arises by the irreversible evolution of some transformation microstructure. For example, on cooling through a second-order transition, the first microstructure might be fine-scale domains which then coarsen as the temperature is lowered. On reheating, the microstructure would not necessarily revert to the finer scale. Any contribution from ferroelastic domain walls can be ruled out in the case of AS

because any that develop during crystal growth appear to be strongly pinned at temperatures up to at least 313 K [24]. Changes in the ferrielectric domain configuration must occur but should not result directly in changes in values of elastic moduli since there is no change in the number of independent moduli across a transition between crystals which are both orthorhombic. Poling of ferrielectric domains would cause changes in bulk piezoelectric moduli, and these would contribute to changes in acoustic resonance frequencies. It is not clear how changes in net electric polarization would occur in the instrument used for RUS measurements, unless the ferrielectric domain sizes are sufficiently large that an imbalance of domain orientations occurs within a crystal, depending on its thermal history.

The changes in local configurations of NH_4^+ and SO_4^{2-} orientations referred to above could be associated with changes in the sizes and distribution of ferrielectric domains as a function of temperature, in the absence of an electric field. This mechanism does not apply in the stability field of the paraelectric structure unless there is a microstructure of locally polarized domains as a precursor to the ferrielectric transition.

C. Chemical decomposition

The change of Crystal #10 from a translucent single crystal with well-defined extinction positions between crossed polars to a white sample with the same external shape and high birefringence at all orientations signifies that a reconstructive change in crystal structure had occurred during the RUS measurements above room temperature. The upper temperature limit of 455 K was below the temperature interval starting at ∼475 K where thermogravimetric measurements have previously revealed substantial weight loss during heating of AS crystals [50,51,53,78]. A more sensitive method for identifying the temperature at which chemical decomposition begins is to detect the first release of NH_3, which Kiyoura and Urano [50] found to be ∼373 K. This lower temperature for the onset of chemical decomposition is consistent with optical studies which have shown a new phase starting to grow on the surface of AS crystals at ∼408 K [51,52].

There are conflicting claims in the literature as to the sequence of product phases that result from heating AS crystals. Kiyoura and Urano [50] proposed that breakdown to AHS + NH_3 takes place between 373 and 443 K, and breakdown to NH_4HSO_4 + NH_3 occurs above 443 K; while Lee *et al.* [52] proposed that the formation of NH_4HSO_4 sets in at 403–425 K, and AHS develops at higher temperatures than this. The presence of acoustic anomalies in Figs. 9 and 10 at temperatures corresponding to known transition temperatures of AHS indicates that the decomposition of Crystal #10 at temperatures up to 455 K was mainly AS → AHS + NH_3. This would give a weight loss of 6.4% if it went to completion, so the observed loss of 2.6 ± 1.2% corresponds to ∼20−60% conversion. Residual AS presumably remained in the core of the sample, with AHS and microcracks forming an outer layer.

D. Elastic properties of AHS

Recovery of a mechanically robust sample from decomposition of Crystal #10 at high temperatures has allowed observation of elastic anomalies accompanying phase transitions in AHS, notwithstanding the presence of microcracks and admixture with AS. Cracks can have a range of effects on RUS spectra. If they are loose enough to allow the sample to behave as multiple resonators, the spectra will contain many more peaks than before they developed, as seen in Fig. 3(a). If cracks have tips which move back and forth under the low dynamic stress that applies in natural resonances at frequencies of ∼0.1−1 MHz, they will give rise to acoustic loss and associated softening. If they do not move, they can be responsible for some degree of softening due simply to a reduction in density of the bulk sample. This limits the confidence with which anomalies in elastic properties shown in Fig. 10 can be understood in detail, beyond correlation with known transition behavior from other studies.

In the summary of Sohn *et al.* [62] (following Refs. [54,55,57,60]), a transition sequence was given for AHS as

$$\mathrm{I}\,(R\bar{3}m) \leftrightarrow \mathrm{II}\,(C2/c) \leftrightarrow \mathrm{III}(P2/n) \leftrightarrow \mathrm{IV}(P2/n) \leftrightarrow \mathrm{V}(P\bar{1}) \leftrightarrow \mathrm{VII}(P1).$$

Based on determination of lattice parameters, the improper ferroelastic I ↔ II transition is first order, with a discontinuity in e_{13} of ∼0.006 at the transition point ∼413 K [57]. Schwalowsky *et al.* [57] also found that the ferroelastic domains in phase II could not be switched by application of an external stress, implying that the walls are strongly pinned. Pinning of the domain walls explains the observation of only slight increases in Q^{-1} below the transition (Fig. 10), in marked contrast with superattenuation that is characteristic of high domain wall mobility below the $Pm\bar{3}m \leftrightarrow R\bar{3}c$ transition in $LaAlO_3$ [79,80].

The II ↔ III transition occurs at ∼265 K and is thermodynamically continuous [56,62]. It does not include the development of a symmetry-breaking shear strain (coelastic). Calorimetric data in the insert of Fig. 11 show an anomaly characteristic of a continuous transition at ∼267 K in Crystal #10 after decomposition in the RUS cycle above room temperature. Steep softening below ∼265 K seen in Fig. 10(a) is presumably due to this transition during the first cooling sequence of Crystal #10, but the data from subsequent heating and cooling are very different. The suspicion must be that the magnitude of the irreversible softening, by up to ∼80%, reflects changes in crack configurations rather than in microstructure or classical strain/order parameter coupling.

The III ↔ IV and IV ↔ V transitions occur within a few degrees on either side of 140 K and, according to Sohn *et al.* [62], are second-order and first-order, respectively. Data from Crystal #10 show only small changes in f^2 and a weak peak in Q^{-1} in this temperature range. There is thus no overt evidence that any ferroelastic domain walls that might be present in crystals with the $P\bar{1}$ structure could be mobile at RUS frequencies.

The lowest temperature transition, V ↔ VII, has been reported to occur at 46 K during cooling and 78 K during heating [55] or 70 K during cooling and 85 K during heating [62]. RUS data in Fig. 10 do not show anomalies which match exactly with these, though there are clear hysteretic changes. Here, f^2 variations with temperature during cooling

and subsequent heating are quite distinct in this temperature range, but both show a distinct break in slope at 72 K. Marked increases in Q^{-1} below ~75 K define a peak that could signify freezing at ~30−40 K of some microstructure in AHS. However, the convergence of resonance frequencies below 30−40 K is present in the data for AS (Fig. 7), and the volume strain of AS also shows leveling off to almost zero slope below ~30 K [Fig. 2(b)]. Further data from samples containing only one phase would be needed at these temperatures to discriminate between phase transitions and freezing of microstructures or other dynamic effects in AS and AHS.

VI. SUMMARY AND CONCLUSIONS

Nonstandard variations of spontaneous strains and elastic properties associated with the ferrielectric transition in AS have been rationalized in terms of bilinear coupling between two order parameters with the same symmetry but different relaxation dynamics and coupling with the ferroelastic order parameter. Additional elasticity data for AHS show that there are more general characteristics of phase transitions in materials which have displacive instabilities that depend also on changes in hydrogen bonding. Hysteretic variations may be anticipated because nonequilibrium combinations of order parameters for displacive and order/disorder components can develop as a direct consequence of their different kinetics.

Displacive components should evolve on a phonon time scale, while order/disorder components are subject to a thermal activation step and will therefore evolve at a rate that may be strongly temperature dependent. The existence of two separate driving mechanisms will also lead to a diversity of transition sequences, depending particularly on differences between their critical temperatures and the strength of coupling between them. In this context, coupling of each order parameter with strain will determine the strength of bilinear coupling via overlapping strain fields. A strain-related mechanism can also account for coupling of ferrielectric order parameters in AS with the order parameter for the ferroelastic transition which occurs at a higher temperature.

Switching of these materials in response to an external field will depend on the dynamics of ferrielectric and ferroelastic domain walls. All the evidence points to ferroelastic domain walls in AS and AHS being strongly pinned, again consistent with the additional role of hydrogen bonding which would have to change across them. Changes in hydrogen bonding would also occur across ferroelectric domain walls, giving them characteristics, particularly with respect to freezing, that would be expected to differ from domain walls in more typical oxide ferroelectrics. In this context, dielectric spectroscopy measurements at low temperatures would help to clarify the mechanisms responsible for freezing behavior in AS and AHS seen from acoustic measurements at the lowest temperatures.

ACKNOWLEDGMENTS

RUS facilities in Cambridge were established through grants from the Natural Environment Research Council (Grants No. NE/B505738/1 and No. NE/F017081/1) and the Engineering and Physical Sciences Research Council (Grant No. EP/I036079/1) to M.A.C.. M.B.C. has received funding from the European Union's Horizon 2020 research and innovation programme under Marie-Sklodowska-Curie Grant Agreement No. 861046. X.M. acknowledges funding from ERC Starting Grant No. 680032 and the Royal Society.

[1] E. Stern-Taulats, T. Castán, Ll. Mañosa, A. Planes, N. D. Mathur, and X. Moya, MRS Bull. **43**, 295 (2018).
[2] X. Moya, S. Kar-Narayan, and N. D. Mathur, Nat. Mater. **13**, 439 (2014).
[3] X. Moya and N. D. Mathur, Science **370**, 797 (2020).
[4] P. Lloveras, E. Stern-Taulats, M. Barrio, J.-Ll. Tamarit, S. Crossley, W. Li, V. Pomjakushin, A. Planes, Ll. Mañosa, N. D. Mathur, and X. Moya, Nat. Commun. **6**, 8801 (2015).
[5] S. Crossley, W. Li, X. Moya, and N. D. Mathur, Phil. Trans. R. Soc. A **374**, 20150313 (2016).
[6] B. T. Matthias and J. P. Remeika, Phys. Rev. **103**, 262 (1956).
[7] S. Hoshino, K. Vedam, Y. Okaya, and R. Pepinsky, Phys. Rev. **112**, 405 (1958).
[8] H.-G. Unruh, Solid State Commun. **8**, 1951 (1970).
[9] E. J. Schlemper and W. C. Hamilton, J. Chem. Phys. **44**, 4498 (1966).
[10] A. Sawada, S. Ohya, Y. Ishibashi, and Y. Takagi, J. Phys. Soc. Jpn. **38**, 1408 (1975).
[11] A. Onodera, Y. Sugata, and Y. Shiozaki, Solid State Commun. **27**, 243 (1978).
[12] J. Petzelt, J. Grigas, and I. Mayerova, Ferroelectrics **6**, 225 (1974).
[13] L. M. Malec, M. Gryl, and K. M. Stadnicka, Inorg. Chem. **57**, 4340 (2018).
[14] B. E. Meijer, G. Cai, F. Demmel, H. C. Walker, and A. E. Phillips, Phys. Rev. B **106**, 064302 (2022).
[15] L. M. Malec, M. Z. Brela, and M. Stadnicka, Acta Mater. **209**, 116782 (2021).
[16] S. Yuan, B. E. Meijer, G. Cai, R. J. C. Dixey, F. Demmel, M. T. Dove, J. Liu, H. Y. Playford, H. C. Walker, and A. E. Phillips, Adv. Funct. Mater. **32**, 2207717 (2022).
[17] H. T. Stokes, D. M. Hatch, and B. J. Campbell, ISOTROPY Software Suite, iso.byu.edu.
[18] M. A. Carpenter, E. K. H. Salje, and A. Graeme-Barber, Eur. J. Mineral. **10**, 621 (1998).
[19] M. A. Carpenter, E. K. H. Salje, A. Graeme-Barber, B. Wruck, M. T. Dove, and K. S. Knight, Am. Mineral. **83**, 2 (1998).
[20] G. Gattow, Acta Cryst. **15**, 419 (1962).
[21] T. Watanabe, K. Sakai, and S. Iwai, Acta Cryst. A **28**, Supplement, S187 (1972).
[22] S. Shiozaki, A. Sawada, Y. Ishibashi, and Y. Takagi, J. Phys. Soc. Jpn. **43**, 1314 (1977).
[23] D. A. Kosova, A. L. Emelina, and M. A. Bykov, Thermochim. Acta **595**, 61 (2014).
[24] Y. Makita, A. Sawada, and Y. Takagi, J. Phys. Soc. Jpn. **41**, 167 (1976).
[25] A. Sawada, Y. Makita, and Y. Takagi, J. Phys. Soc. Jpn. **41**, 174 (1976).

[26] R. Docherty, A. El-Korashy, H.-D. Jennissen, H. Klapper, K. J. Roberts, and T. Scheffen-Lauenroth, J. Appl. Cryst. **21**, 406 (1988).
[27] K. Hasebe, J. Phys. Soc. Jpn. **50**, 2660 (1981).
[28] I. M. Shmyt'ko, N. S. Afonikova, and V. I. Torgashev, Phys. Solid State **44**, 2309 (2002).
[29] T. Asahi, R. Ikeda, M. Nakamura, T. Morikawa, M. Higano, H. Suzuki, and J. Kobayashi, Ferroelectrics **21**, 47 (1996).
[30] M. A. Carpenter, H.-W. Meyer, P. Sondergeld, S. Marion, and K. S. Knight, Am. Mineral. **88**, 534 (2003).
[31] M. A. Carpenter, J. F. J. Bryson, G. Catalan, and C. J. Howard, J. Phys.: Condens. Matter **24**, 045901 (2012).
[32] A. Migliori and J. L. Sarrao, *Resonant Ultrasound Spectroscopy: Applications to Physics, Material Measurements, and Nondestructive Evaluation* (Wiley, New York, 1997).
[33] R. E. A. McKnight, T. Moxon, A. Buckley, P. A. Taylor, T. W. Darling, and M. A. Carpenter, J. Phys.: Condens. Matter **20**, 075229 (2008).
[34] J. Schiemer, L. J. Spalek, S. S. Saxena, C. Panagopoulos, T. Katsufuji, A. Bussmann-Holder, J. Köhler, and M. A. Carpenter, Phys. Rev. B **93**, 054108 (2016).
[35] D. M. Evans, J. A. Schiemer, M. Schmidt, H. Wilhelm, and M. A. Carpenter, Phys. Rev. B **95**, 094426 (2017).
[36] A. Aznar, P. Lloveras, J.-Y. Kim, E. Stern-Taulats, M. Barrio, J. Ll. Tamarit, C. F. Sánchez-Valdés, J. L. Sánchez Llamazares, N. D. Mathur, and X. Moya, Adv. Mater. **31**, 1903577 (2019).
[37] T. Ikeda, K. T. Fujibayashi, T. Nagai, and J. Kobayashi, Phys. Stat. Sol. (a) **16**, 279 (1973).
[38] H. Hussinger and H.-G. Unruh, Phys. Stat. Sol. (a) **44**, 525 (1977).
[39] H. L. Bhat, G. F. Clark, H. Klapper, and K. J. Roberts, J. Phys. D: Appl. Phys. **28**, A23 (1995).
[40] H. L. Bhat, H. Klapper, and K. J. Roberts, J. Appl. Cryst. **28**, 168 (1995).
[41] M. A. Carpenter and E. K. H. Salje, Eur. J. Mineral. **10**, 693 (1998).
[42] A. Yoshihara, T. Fujimara, and K.-I. Kamiyoshi, J. Phys. Soc. Jpn. **44**, 1241 (1978).
[43] H.-G. Unruh, E. Sailor, H. Hussinger, and O. Ayere, Solid State Commun. **25**, 871 (1978).
[44] N. Nakanishi, Y. Murakami, M. Tobiaka, H. Sugiyama, and S. Kachi, J. Phys. Soc. Jpn. **35**, 947 (1973).
[45] S. A. Gridnev, L. P. Safonova, and O. N. Ivanov, and T. N. Davydova, Phys. Solid State **40**, 1998 (1998).
[46] W. Rehwald, A. Vonlanthen, J. K. Krüger, R. Wallerius, and H.-G. Unruh, J. Phys. C: Solid State Phys. **13**, 3823 (1980).
[47] W. Rehwald and A. Vonlanthen, Solid State Commun. **38**, 209 (1981).
[48] T. K. Song, S.-M. Lee, and S.-I. Kwun, J. Phys. Soc. Jpn. **62**, 1409 (1993).
[49] Y.-H. Kim, B.-G. Kim, and J.-J. Kim, J. Phys. Soc. Jpn. **65**, 304 (1996).
[50] R. Kiyoura and K. Urano, Ind. Eng. Chem. Process Des. Dev. **9**, 489 (1970).
[51] K.-S. Lee, J.-L. Kim, H.-T. Jeong, and S.-Y. Jeong, J. Korean Phys. Soc. **29**, Proc. Supplement S424 (1996).
[52] K.-S. Lee, I.-H. Oh, and J.-H. Ko, J. Solid State Chem. **212**, 107 (2014).
[53] H. Muroyama, T. Matsui, R. Kikuchi, and K. Eguchi, Solid State Ionics **176**, 2467 (2005).
[54] K. Gesi, Phys. Stat. Sol. (a) **33**, 479 (1976).
[55] K. Gesi, Jpn. J. Appl. Phys. **19**, 1051 (1980).
[56] D. S. Babu, G. S. Sastry, M. D. Sastry, and A. G. I. Dalvi, J. Phys. C: Solid State Phys. **18**, 6111 (1985).
[57] L. Schwalowsky, U. Bismayer, and T. Lippmann, Phase Trans. **59**, 61 (1996).
[58] K. Friese, M. I. Aroyo, L. Schwalowsky, G. Adiwidjaja, and U. Bismayer, J. Solid State Chem. **165**, 136 (2002).
[59] L. Schwalowsky, V. Vinnichenko, A. Baranov, U. Bismayer, B. Merinov, and G. Eckold, J. Phys.: Condens. Matter **10**, 3019 (1998).
[60] R. H. Chen, T. M. Chen, and C. S. Shern, J. Phys. Chem. Solids **61**, 1399 (2000).
[61] P. M. Dominiak, J. Herold, W. Kolodziejski, and K. Wozniak, Inorg. Chem. **42**, 1590 (2003).
[62] Y. J. Sohn, K. M. Sparta, S. Prinz, M. Meven, G. Roth, and G. Heger, Acta Cryst. B **69**, 336 (2013).
[63] D. A. Kosova, A. I. Druzhinina, L. A. Tiflova, A. S. Monayenkova, E. V. Belyaeva, and I. A. Uspenskaya, J. Chem. Thermodyn. **132**, 432 (2019).
[64] D. Swain, V. S. Bhadram, P. Chowdhury, and C. Narayana, J. Phys. Chem. A **116**, 223 (2012).
[65] J. E. Diosa, M. E. Fernández, and R. A. Vargas, Phys. Stat. Sol. (b) **227**, 465 (2001).
[66] O. Björkström, A. Fredricksson, B.-E. Mellander, J. E. Diosa, and R. A. Vargas, Solid State Ionics **69**, 75 (1994).
[67] E. A. Mikhaleva, I. N. Flerov, A. V. Kartashev, M. V. Gorev, E. V. Bogdanov, and V. S. Bondarev, Solid State Sci. **67**, 1 (2017).
[68] S. Jerzak, Ferroelectrics **200**, 197 (1997).
[69] E. Salje, Phys. Chem. Minerals **12**, 93 (1985).
[70] E. Salje, B. Kuscholke, B. Wruck, and H. Kroll, Phys. Chem. Minerals **12**, 99 (1985).
[71] E. Salje and V. Devarajan, Phase Trans. **6**, 235 (1986).
[72] M. A. Carpenter, Thermochemistry of aluminium/silicon ordering in feldspar minerals, in *Physical Properties and Thermodynamic Behaviour of Minerals*, edited by E. K. H. Salje (Springer, Dordrecht, 1988), p. 265.
[73] A. Sawada, Y. Takagi, and Y. Ishibashi, J. Phys. Soc. Jpn. **34**, 748 (1973).
[74] K. Hasebe and S. Tanisaki, J. Phys. Soc. Jpn. **42**, 568 (1977).
[75] M. Fujimoto, L. A. Dressel, and T. J. Yu, J. Phys. Chem. Solids **38**, 97 (1977).
[76] D. De Sousa Meneses, G. Hauret, P. Simon, F. Bréhat, and B. Wyncke, Phys. Rev. B **51**, 2669 (1995).
[77] D. E. O'Reilly and T. Tsang, J. Chem. Phys. **46**, 1291 (1967).
[78] A. El-Korashy and G. A. Mohamed, Ferroelectrics **124**, 385 (1991).
[79] M. A. Carpenter, A. Buckley, P. A. Taylor, and T. W. Darling, J. Phys.: Condens. Matter **22**, 035405 (2010).
[80] M. A. Carpenter, J. Phys.: Condens. Matter **27**, 263201 (2015).